BNL-224614-2023-JAAM

First-Principles Study of n-Butane Monomolecular Cracking and Dehydrogenation on Two-Dimensional-Zeolite Model Systems: Reaction Mechanisms and Effects of Spatial Confinement

M. Wang, D. Lu

To be published in "The Journal of Physical Chemistry C"

July 2023

Center for Functional Nanomaterials

Brookhaven National Laboratory

U.S. Department of Energy

USDOE Office of Science (SC), Basic Energy Sciences (BES) (SC-22)

DISCLAIMER

First-principles Study of *n*-butane Monomolecular Cracking and dehydrogenation on 2D-Zeolite Model Systems: Reaction Mechanisms and Effects of Spatial Confinement

Mengen Wang[1,2,3], Jorge Anibal Boscoboinik[1] and Deyu Lu[1*]*

[1] Center for Functional Nanomaterials, Brookhaven National Laboratory, Upton, NY 11973, United States.

[2] Materials Science and Chemical Engineering Department, Stony Brook University, Stony Brook, NY 11790, United States.

KEYWORDS Butane cracking; Reaction pathway; Confinement effect; Zeolite; Aluminosilicate bilayer film; Density functional theory

ABSTRACT Two-dimensional (2D) ultrathin (~0.5 nm) aluminosilicate bilayer films, consisting of hexagonal prisms (a.k.a. double 6-membered rings D6R) with acidic bridging hydroxyl groups exposed on the surface, have been previously synthesized on a Ru(0001) surface as a zeolite model system. These structures are helpful for mimicking zeolite catalysts with D6R building blocks, such as chabazite. We performed density functional theory calculations to investigate the monomolecular cracking and dehydrogenation of *n*-butane molecules over the acidic hydroxyl groups of the 2D model system and compared the reaction energetics with that in bulk chabazite. The intrinsic activation energy barrier is the highest for dehydrogenation and lowest for central C-

[3] Current Affiliation: Department of Electrical and Computer Engineering, Binghamton University, Binghamton, NY 13850, United States

C bond cracking in bulk chabazite. The trend of intrinsic energy barriers for dehydrogenation, terminal and central C-C bond cracking is reproduced on the 2D aluminosilicate film. Overall, the activation barriers are higher on the 2D film than in bulk chabazite due to the lack of confinement in the former. We further explored the effects of the zeolite channel size on the *n*-butane adsorption and monomolecular cracking using different bulk nanoporous zeolite frameworks (TON, MEL, MEI, and VFI). We found that as the confinement of channels decreases, *n*-butane adsorption becomes weaker, and the intrinsic energy barrier of terminal C-C cracking increases. The activation energy barriers (dehydrogenation, terminal and central C-C cracking) on the 2D bilayer film surface, which may be considered as zeolite cages at the infinite cage size limit, are close to that in VFI with a relatively large channel size. Comparing the reaction pathway of *n*-butane terminal C-C cracking in 3D nano-cages and on the surface of the 2D aluminosilicate film revealed that stabilizing the transition states in the 3D nano-cages is responsible for the decrease in the intrinsic energy barriers for bulk zeolites.

1. Introduction

Zeolites are widely used industrial catalysts with nanoporous structures consisting of [AlO_4^-] and [SiO_4] tetrahedra. Their channels are ideal for adsorbing molecules and hosting high density of active sites[1-6]. There are more than 200 identified framework structures of zeolites[7]. Among different zeolite structures, the variation in channel sizes provides different degree of confinement to relevant chemical processes (e.g., absorption, reaction and desorption). Chabazite is one of the common types of zeolite, where 6-member rings (6MRs) and 8-member rings (8MRs) are present[8]. The catalytically active hydroxyl group sites are located in the 8MR. As the active sites in bulk nano-porous structures are inaccessible for surface science measurements, typically used for detailed mechanistic studies, a well-defined 2D model zeolite framework with hydroxyl groups

exposed on the surface has been synthesized previously, providing opportunities for mechanistic surface science studies of reactions catalyzed by Brønsted acid sites[9, 10].

There have been intensive research efforts devoted to these 2D silicate bilayer films. The electronic properties of silica bilayer/Ru heterojunctions[11, 12] were studied, and the heterojunctions were proposed for trapping Ar, Kr, Xe and CO[13-15]. Au and Pd atoms were deposited on the silica film, in an attempt to study the catalytic properties of Pd nano-clusters on silica film[16]. The interactions between molecules (CO and C_2H_4) and the exposed hydroxyl groups from (Si-OH-Al) were also studied by Infrared Reflection-Absorption Spectroscopy (IRAS) and density functional theory (DFT) to compare the properties of hydroxyl groups in 3D and 2D zeolites[10]. The aluminosilicate bilayer (zeolite model system) has the same tetrahedral [SiO_4] and [AlO_4^-] building blocks and D6R secondary building units as chabazite. However, the catalytic properties of the 2D-zeolite model system have not been fully understood.

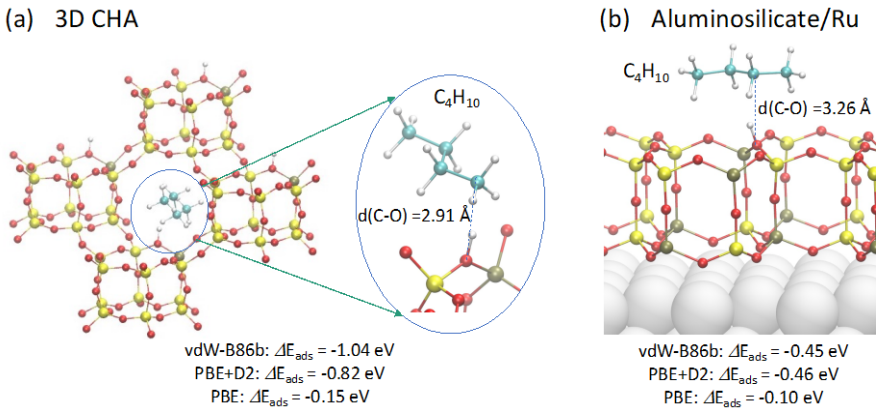

Figure 1. Atomic structures of *n*-butane adsorbed (a) in the nano-cage of chabazite ($HAlSi_{11}O_{24}$) and (b) on the bilayer aluminosilicate film ($HAl_3Si_5O_{16}$). Color code: Si (yellow), Al (grey), O (red), C (cyan), and H (white).

A major difference between the 3D CHA with the 2D aluminosilicate is the degree of the confinement around the active site (Brønsted acid). Figure 1 shows the atomic structures of butane

molecule adsorbed within a chabazite pore [Figure 1(a)] and on the bilayer aluminosilicate surface [Figure 1(b)]. Chemical reactions take place within the small pore in 3D CHA, while the 2D aluminosilicate can be treated as having an infinitely large pore. The pore size can have a significant effect on the catalytic activity of zeolite. However, the atomic level details are still lacking. For example, a change in the pore size can affect the interaction between the pore and small molecules trapped inside. As far as the pore size is larger than the van der Waals (vdW) radius of the trapped molecules, a smaller pore size leads to larger vdW interactions between the absorbate and the pore, which results in a more negative adsorption energy and therefore helps to stabilize the molecular species in the chemical reaction. One may argue that such a confinement effect should apply to both the adsorbed state and the transition state, the net effect of the nano-cage does not alter the intrinsic activation energy barrier (E_a), which is defined as the energy difference between the adsorbed state and the transition state. However, recent experimental and quantum mechanics/molecular mechanics (QM/MM) studies reveal that the confinement effect of zeolite nano-cages with different pore sizes can modify both the adsorption energy of butane molecules and the intrinsic butane cracking and dehydrogenation energy barriers[17, 18]. Therefore, it is important to gain insight on the confinement effect of 2D/3D zeolites at atomic level using first principles methods.

We focus on the monomolecular cracking and dehydrogenation of the *n*-butane molecule as an exemplary case to compare the reaction mechanism on the 2D aluminosilicate films and in bulk chabazite. We discuss the adsorption geometry and energy of a butane molecule and determine the reaction pathway and E_a of butane dehydrogenation and cracking. Our results show that the 2D zeolite model system could reproduce the trend in E_a compared with bulk chabasite. We further

compare E_a of butane cracking in VFI, MEI, MEL, and TON with various channel sizes to quantify the confinement effect.

2. Computational methods

DFT calculations were performed using the projector augmented wave method implemented in the Vienna Ab initio simulation package (VASP)[19, 20]. The vdW-b86B functional was used to treat the non-local vdW interactions[21-23]. The 2D-zeolite model system consists of the aluminosilicate bilayer adsorbed on 3 layers of Ru atoms in a 10.784 Å × 9.339 Å × 27 Å cell. The Brillouin zone was sampled with 2×2×1 and a kinetic energy cutoff of 800 eV was used. The aluminosilicate bilayer, chemisorbed O atoms and top two layers of Ru atoms were allowed to relax in the structural optimization until forces were smaller than 0.01 eV/Å. The initial atomic structures of the bulk zeolite are taken from the zeolite database.[7] One Si atom inside the nano-channel is replaced by an Al atom to build the aluminosilicate bilayer model, following the procedure established in our previous work[12]. All atoms and the unit cell size were allowed to relax in the structural optimization for bulk zeolite.

The reaction pathways and energy barriers are calculated using the climbing image nudged elastic band method (CI-NEB)[24] implemented in VASP. The silica bilayer, chemisorbed O atoms and top two layers of Ru atoms were allowed to relax in the CI-NEB calculations until forces were smaller than 0.03 eV/Å. To obtain the free energy for intrinsic activation (G_a) along the reaction pathway, we calculated the vibrational contribution to the internal thermal energy (E_v) and entropy (S_v) (supporting information).[25] The vibrational frequencies are calculated using the finite differences method implemented in VASP with the displacement step size of 0.015 Å. The H atom

from the zeolite framework and the butane molecule are allowed to move and the zeolite frameworks are kept fixed during the vibrational frequency calculations.

3. Results and discussions

3.1 Butane adsorption, dehydrogenation and monomolecular cracking over the 2D-zeolite model

Butane molecules have multiple adsorption orientations on the aluminosilicate film. Four different adsorption orientations (Figure S1) are compared, which were made possible by rotation and translation of the butane molecules. The adsorption energy is defined as $\Delta E_{ads} = E_{zeo+butane} - E_{zeo} - E_{butane}$, where the energies are calculated for relaxed structures of the whole system and subsystems of 2D-zeolite model and a butane molecule. ΔE_{ads} of the four configurations are close to each other (within 0.07 eV), indicating that the absorbed butane molecules may adopt different rotation angles on the aluminosilicate bilayer surface. The orientation of Conf. 4 shown in Figure S1 is chosen as the initial state for the following discussions as it results in both lower adsorption energy (ΔE_{ads}) and lower intrinsic activation energy barrier for dehydrogenation (E_a) than other orientations.

Monomolecular cracking and dehydrogenation of alkane molecules occur at very low conversion where the Brønsted acid sites are mostly unoccupied.[26, 27] The reaction mechanism and reaction rates in different zeolite frameworks have been reported.[17, 18] Monomolecular cracking mechanisms of alkane molecules in zeolites has been widely studied from theoretical calculations[26, 28, 29] and experiments[30]. The reaction mechanism of butane cracking and dehydrogenation is illustrated in Scheme 1.[29] In dehydrogenation, the C-H bond interacts with the

proton from the Brønsted acid site to produce H_2 and butene (C_4H_8). There are two different types of C-C bonds in butane: the terminal C-C bond and the central C-C bond. Terminal cracking of C_4H_{10} produces CH_4 and C_3H_6, while central cracking produces C_2H_6 and C_2H_4.

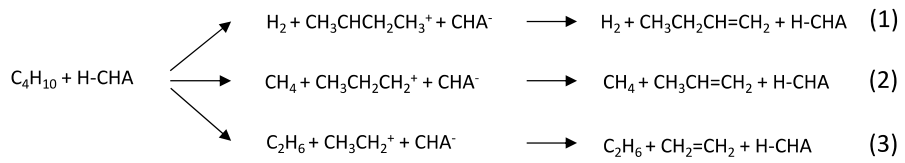

Scheme 1. Reaction pathways of *n*-butane dehydrogenation (1), terminal C-C cracking (2), and central C-C bond cracking (3).

We start with discussing the dehydrogenation reaction of *n*-butane. The minimum energy pathway for the dehydrogenation is calculated using the CI-NEB method and the corresponding transitions state (TS1) and the final state (FS1) is illustrated in Figure 2 (a) and (b). During the reaction, the proton from the hydroxyl group breaks the C-H bond in the internal methylene group and combines with the hydrogen to form a hydrogen molecule, leaving a carbocation ($C_4H_9^+$) with the negatively charged aluminosilicate bilayer ($Al_3Si_5O_{16}^-$). Then the proton from $C_4H_9^+$ is detached from the molecule and bonds to the O atom in $Al_3Si_5O_{16}^-$ re-forming the hydroxyl group. The product is a butene molecule and a hydrogen molecule with E_a of 2.26 eV. The butane dehydrogenation on 2D silicate film features a late transition state, where the H_2 molecule is nearly formed, which is also consistent with butane cracking on other zeolite frameworks.[29] We also explored the reaction when the proton attacks the C-H bond from the terminal methyl group and found an E_a of 2.65 eV, which is a less preferred pathway. This is consistent with Ref.[29] that shows the butane dehydrogenation prefers the methylene pathway over the methyl group on MFI.

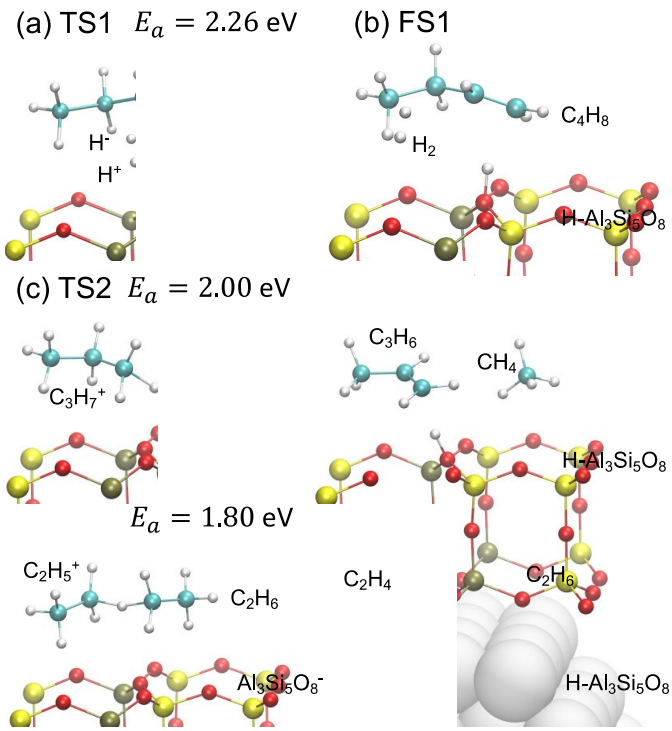

Figure 2. The structures of the transition states and final states geometries for dehydrogenation (a, b), terminal cracking (c, d), and central cracking (e, f). Color code: Si (yellow), Al (grey), O (red), C (cyan), and H (white).

The rate limiting step in terminal monomolecular cracking is associated with the proton from hydroxyl groups breaking the terminal C-C bond [Figure 2(c)] to form a methane (CH_4) and a propene (C_3H_6) molecule [Figure 2(d)]. E_a in this reaction is 2.00 eV, which is 0.26 eV lower than the dehydrogenation. When the hydrogen molecule breaks the central C-C bond [Figure 2(e)], it leads to the formation of an ethane molecule and a $C_2H_5^+$ cation, which eventually loses a proton and forms an ethylene molecule [Figure 2(f)], with an even lower E_a of 1.80 eV. We determine the transition state to be the protonation of the butane molecules where the C-H-C bonding forms [Figure 2(c) and 2(e)]. The same transition states were discovered for butane terminal and central cracking in MFI[29, 31] and H-ZSM-5[32]. A similar mechanism was also reported for propane cracking where the transition state is associated with the direct attacking of H from the zeolite frameworks

to the C-C bond[31-33]. Propane cracking on the freestanding 2D aluminosilicate was investigated in Ref.[33], where the C-H-C transition state was not identified and a lower activation barrier was reported as compared to the FAU framework. We note that besides the difference in butane and propane cracking, the freestanding bilayer model used in Ref.[33] with a relatively low Al/Si ratio (1/47) could also play a nontrivial role in determining the transition states and activation barriers. These aspects are worth further exploration in future works.

Comparison between 2D aluminosilicate with bulk chabazite

In the prevision section, we have discussed the reactions on the 2D aluminosilicate bilayer. It is important to compare the reaction barriers in the 2D aluminosilicate model system with those in bulk chabazite. The butane molecules are adsorbed within the pores of chabazite close to the OH group. Due to the confinement effect from the nano-cages, the butane molecule is closer to the framework in bulk chabazite, at a distance of 2.91 Å compared to the 3.26 Å in the 2D-zeolite model. The butane-aluminosilicate distance is defined as the distance between the O atom from the OH group in zeolites and the closest C atom to the aluminosilicate film ($d_{C\text{-}O}$). As shown in Figure 1, ΔE_{ads} of the bulk chabazite is -1.04 eV while ΔE_{ads} of the 2D aluminosilicate film is -0.45 eV. The relation between $d_{C\text{-}O}$ and ΔE_{ads} suggests that the confinement effect of the bulk chabazite stabilizes the adsorbed butane molecule. The PBE-D2[34] functional and the PBE[35, 36] functional were also used to calculated ΔE_{ads}. As shown in Figure 1, the adsorption energy of butane in bulk chabazite using the PBE+D2 functional is -0.82 eV, which is 0.36 eV lower than the 2D aluminosilicate bilayer (ΔE_{ads} = -0.46 eV). PBE functional yields a much smaller ΔE_{ads}, which is -0.15 eV for bulk chabazite and -0.10 eV for 2D aluminosilicate film. The PBE adsorption

energies is similar in 2D and bulk chabazite, meaning that nano-cages of 3D-CHA help stabilize the adsorption of butane via vdW forces.

The free energy for adsorption (ΔG_{ads}) is defined as $\Delta G_{ads} = \Delta H_{ads} - T\Delta S_{ads}$, and the enthalpy of adsorption is calculated as $\Delta H_{ads} = \Delta E_{ads} + \Delta E_v + \Delta PV$, where the vibrational (ΔE_v) contribution to the internal thermal energy and $\Delta PV = -k_BT$ are included.[25] The vibrational contribution is included in the adsorption entropy (ΔS_{ads}). We note that, for alkane adsorption in zeolites, certain rotational and translational degrees of freedom of adsorbed alkane molecules are likely preserved, which results in a smaller entropy loss as compared to the standard immobile physisorption picture.[37, 38] In addition, since the main focus of this study is to identify trends of the reaction energetics of *n*-butane monomolecular cracking in zeolite with different pore sizes, the translational and rotational contributions to the free energy of gas phase *n*-butane are the same for all the systems and neglecting them will not affect our conclusion. Therefore, the translational and rotational contributions to the free energies are neglected in this work. The vdW-b86B functional yields ΔH_{ads} = -0.96 eV, $T\Delta S_{ads}$ = -0.15 eV, and ΔG_{ads} = -0.81 eV at 348 K. We note that the calculated ΔH_{ads} = -0.96 eV is lower than the experimental values, which are in the range of -0.47 eV to -0.66 eV in bulk chabazite.[39, 40] The vdW-b86B functional overestimates the adsorption enthalpy while the adsorption energy predicted by the PBE-D2 functional agrees better with the experimental values, which is consistent with the trend in the adsorption energies of shorter alkane molecules in chabazite[41, 42]. As one focus of our study includes the Ru/aluminosilicate system, we adopted the vdW-b86B functional, which reproduces well the experimental lattice constants of both bulk Ru and chabazite,[11, 12] and show good agreement with experiments for reactions at the silicate/Ru interface.[43, 44]

The potential energy surface of butane dehydrogenation and monomolecular cracking is summarized in Figure 3 (a). The solid lines represent 2D aluminosilicate film and the dashed lines represent bulk chabazite. The trend in E_a for dehydrogenation and monomolecular cracking is similar in 2D and bulk chabazite. The energy barrier is the highest for dehydrogenation and lowest for central C-C bond cracking. We also included the vibrational contribution to calculate the free energy of intrinsic activation (G_a), which generate the same trends in both 2D aluminosilicate and 3D chabazite, where the intrinsic barrier is the highest for dehydrogenation and lowest for central C-C bond cracking (Figure 3b-3d). This trend is also consistent with previous studies of butane dehydrogenation and cracking calculated by QM/MM in zeolites with different channel size.[17, 29] Due to the confinement effect from the 3D nano-cages, G_a is lowered by 0.40 eV for dehydrogenation, by 0.19 eV for terminal C-C cracking, and by 0.02 eV in central C-C bond cracking. We note that our results are based on static calculations at the semi-local DFT level, and more accurate results may be obtained using *ab initio* molecular dynamics or higher-level methods.[26, 33, 45-47]

It is interesting to point out that while the three reaction pathways are similar in energy for the 3D structure, larger differences are obtained for the 2D case. This would result in potentially higher selectivity toward central C-C bond cracking in the 2D case. For example, for the 3D chabazite structure, the difference in G_a between terminal cracking and dehydrogenation is 0.06 eV while for the 2D-zeolite model this difference is 0.27 eV. This can be understood as the dehydrogenation is more affected by the confinement effect. From the transition state structures shown in Figure 3b-3d, we found that the dehydrogenation features late transition states where H_2 molecules are nearly formed and C-C cracking resembles more of the reactants than the products for both 2D and 3D chabazites. The dehydrogenation reaction is therefore more sensitive to the van der Waals

interaction with the neighboring environment like the pores in zeolite.[9] This is also consistent with butane cracking on other zeolite frameworks.[17, 29]

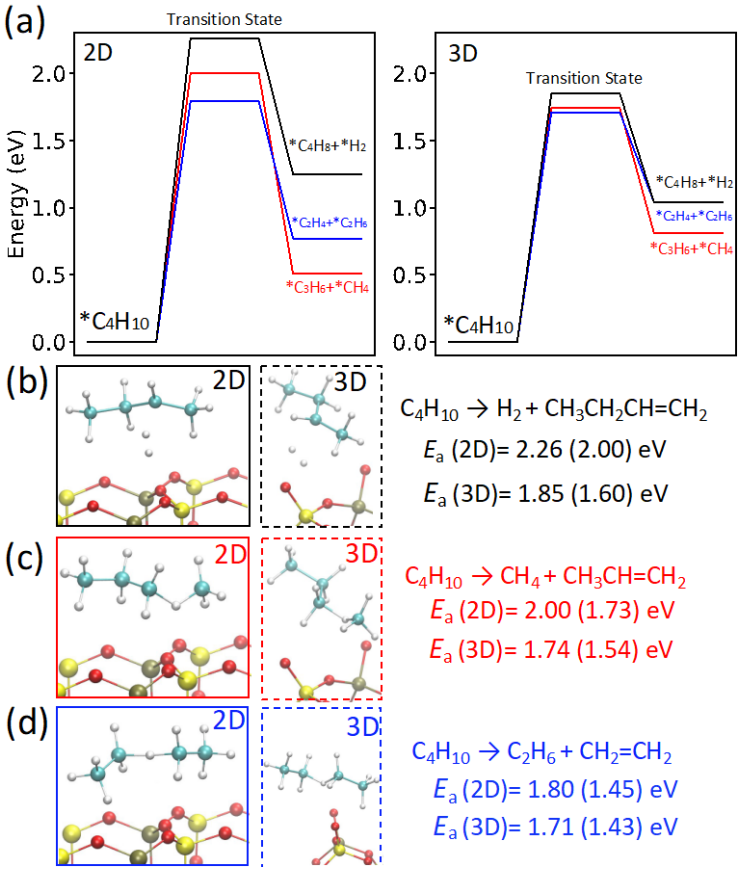

Figure 3. (a) Potential energy surface for butane dehydrogenation and cracking on 2D aluminosilicate (left) and in 3D chabazite (right). Structures of transition states for dehydrogenation (b), terminal C-C bond (c) and central C-C bond cracking (d) in 2D and 3D chabazite. The numbers in parenthesis are the calculated free energies of intrinsic activations (G_a). Color code: Si (yellow), Al (grey), O (red), C (cyan), and H (white).

3.3 Effects of zeolite spatial confinement

As the activation energies for dehydrogenation and cracking of butane are affected by the confinement, we further explored four more zeolite frameworks with different channel sizes (d_{ch}) to quantify the effect from confinement. The adsorption and cracking of butane have been studied on TON and MEL frameworks experimentally.[17] To study a wider range of the confinement effect, we chose two more zeolite frameworks with larger channel sizes (MEI and VFI) that can be experimentally synthesized[48, 49] and have been previously used to study confinement effects via theoretical computations.[50, 51] Figure 4 shows the structures of butane molecules adsorbed in the channels of the zeolites, with the channel sizes increasing from 5.4 Å (TON), 6.2 Å (MEL), 8.1 Å (MEI), to 13.2 Å (VFI). The channel size (d_{ch}) is calculated as $d_{ch} = d_{O\text{-}O} - d_O$, *where* $d_{O\text{-}O}$ is the O-O distance at the opposite sides of the channel and d_O = 1.46 Å is the covalent diameter of the O atom.[52] As the degree of confinement decreases, $d_{C\text{-}O}$ increases from 3.36 Å (TON), 3.51 Å (MEL), 3.68 Å (MEI), to 4.11 Å (VFI). The adsorption energies (ΔE_{ads}), consequently, reduces in magnitude from -1.31 eV (TON), -0.94 eV (MEL), -0.69 eV (MEI), to -0.52 eV (VFI). At a typical reaction temperature T = 673K, the adsorption enthalpy (ΔH_{ads}) is -1.31 eV (TON), -0.93 eV (MEL), -0.68 eV (MEI), and -0.52 eV (VFI). The adsorption entropy calculated at T = 673K ($T\Delta S_{ads}$) is -0.26 eV (TON), -0.25 eV (MEL), -0.23 eV (MEI), and -0.26 eV (VFI). ΔG_{ads} of butane adsorption is -1.05 eV (TON), -0.68 eV (MEL), -0.45 eV (MEI), to -0.26 eV (VFI). d_{ch} and $d_{C\text{-}O}$ are plotted against (ΔE_{ads}) in Figure 5 (a) and 5 (b). The trends can be fitted to $d_{ch} = 186.55e^{6.12\Delta E_{ads}} + 5.44$ (Å) [Figure 5 (a)] and $d_{C\text{-}O} = 7.71e^{4.50\Delta E_{ads}} + 3.36$ (Å) [Figure 5 (b)], which illustrate that the adsorption energy becomes less negative as confinement decreases.

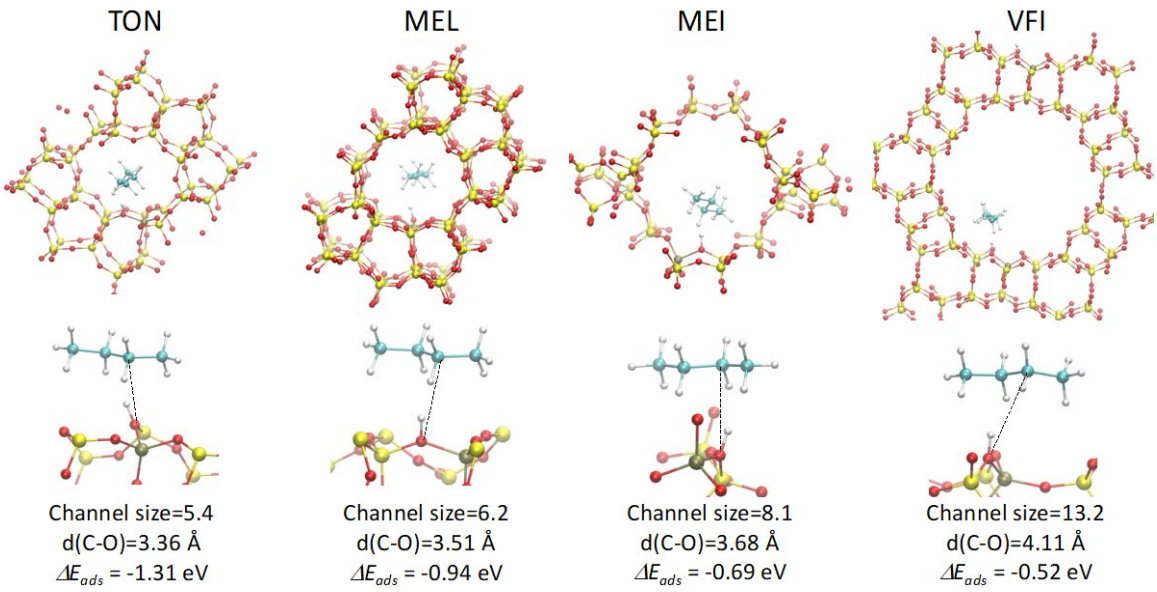

Figure 4. The structures of the adsorbed states for butane molecules in (a) TON, (b) MEL, (c) MEI and (d) VFI. Color code: Si (yellow), Al (grey), O (red), C (cyan), and H (white).

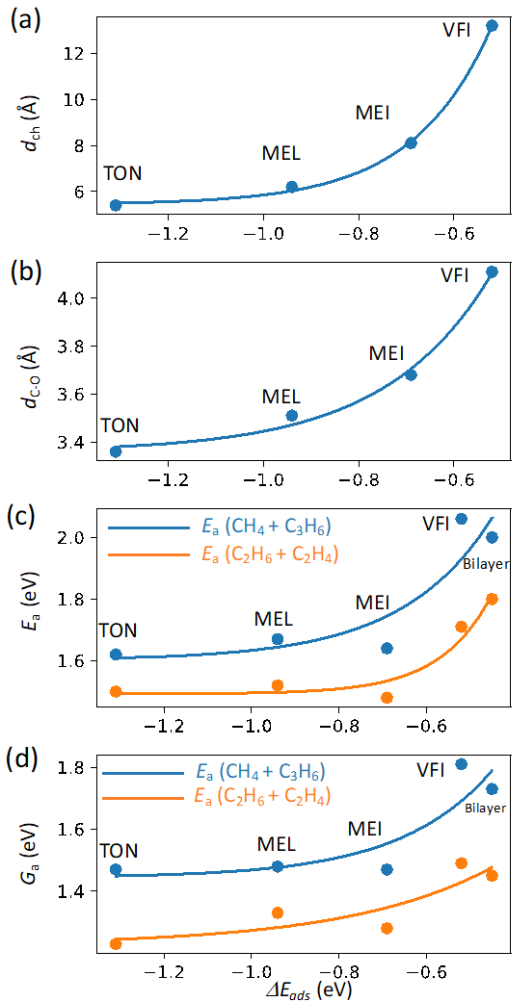

Figure 5. The channel size (d_{ch}) (a), butane-zeolite distance ($d_{C\text{-}O}$) (b), and intrinsic activation energy barriers (c) and free energy of activation (d) for terminal C-C bond cracking (blue) and central C-C bond cracking (orange) plotted against the adsorption energy for TON, MEL, MEI, and VFI.

The activation energies of the terminal and central C-C bond cracking are calculated. Figure S2 shows the transition states for terminal and central C-C bond cracking in different zeolite frameworks studied in this work. The structures are similar in these zeolites, where are carbon cations are formed by a proton detached from hydroxyl groups and adsorbed to the butane

molecule. E_a is plotted against ΔE_{ads} in Figure 5 (c), which decreases from 2.06 eV (VFI), 1.64 eV (MEI), 1.67 eV (MEL) to 1.62 eV (TON) for terminal C-C cracking with fitted curve of $E_a = 4.14e^{4.88\Delta E_{ads}} + 1.60$ (eV) and from 1.71 eV (VFI), 1.48 eV (MEI), 1.52 eV (MEL) to 1.50 eV (TON) for central C-C cracking with fitted curve of $E_a = 14.71e^{8.49\Delta E_{ads}} + 1.49$ (eV). To evaluate the effect from confinement to the free energy of activation, we also plotted G_a evaluated at T = 673 K against ΔE_{ads} in Figure 5 (d). Including the vibrational contribution, the activation enthalpy (H_a) is 1.98 eV (VFI), 1.60 eV (MEI), 1.62 eV (MEL) and 1.57 eV (TON) for terminal C-C cracking and 1.60 eV (VFI), 1.41 eV (MEI), 1.44 eV (MEL) and 1.41 eV (TON) for central C-C cracking. The entropy contribution calculated at T = 673 K is 0.17 eV (VFI), 0.13 eV (MEI), 0.14 eV (MEL) and 0.10 eV (TON) for terminal C-C cracking and 0.11 eV (VFI), 0.13 eV (MEI), 0.11 eV (MEL) and 0.18 eV (TON) for central C-C cracking. G_a decreases from 1.81 eV (VFI), 1.47 eV (MEI), 1.48 eV (MEL) to 1.47 eV (TON) for terminal C-C cracking with fitted curve of $G_a = 2.94e^{4.76\Delta E_{ads}} + 1.44$ (eV) and from 1.49 eV (VFI), 1.28 eV (MEI), 1.33 eV (MEL) to 1.23 eV (TON) for central C-C cracking with fitted curve of $G_a = 0.98e^{3.04\Delta E_{ads}} + 1.23$ (eV). Consistent with the QM/MM result, the central C-C bond cracking is less affected by the confinement effect than the terminal C-C bond[18]. At a channel size greater than MEL, the confinement affects both the adsorption energy and the intrinsic energy barrier. The confinement will reach a plateau under small d_{ch}, where only adsorption energies are slightly affected. This is consistent with previous studies that found the activation enthalpies of frameworks with small channel sizes are not significantly dependent on the confinement effect.[40] The E_a and G_a of butane cracking on 2D-zeolite model system is close to the that of VFI, indicating that the values of intrinsic activation energies from bilayer model system could be compared to zeolites with a relatively large channel or pore sizes.

Conclusion

We studied the reaction mechanisms and activation energy barriers of butane dehydrogenation and monomolecular cracking on a well-defined 2D-zeolite model system using density functional theory. The results are compared with bulk chabazite to understand the role of confinement effects in these reaction pathways. The 2D-zeolite model system reproduces the trend in energy barriers, where the dehydrogenation has the highest barrier and central C-C bond cracking has the lowest barrier. However, the difference in energy barrier between the pathways increases as confinement effects are eliminated for the 2D case. The central C-C bond cracking is less affected by the confinement effect than the dehydrogenation reaction. We further calculated the energy barriers for butane cracking in multiple channels VFI, MEI, MEL, and TON with varying sizes, and we found that the confinement within the bulk zeolites reduces the adsorption energy as well as the intrinsic energy barriers. The activation energy barriers for the 2D-zeolite model are close to those of the VFI framework, which has the largest channel size among the structures addressed in this work.

Supporting Information

See supporting information for additional information about adsorption configurations of butane molecules on aluminosilicate/Ru, structures of the transition states for butane terminal and central cracking, and computational details for the vibrational contribution to the internal thermal energy and entropy.

Corresponding Author

D.L. (dlu@bnl.gov)

M.W. (mengenwang@binghamton.edu)

Author Contributions

All authors participated in discussions, data analysis and manuscript preparation.

Notes

The authors declare no competing financial interests.

ACKNOWLEDGMENTS

Research is carried out using the theory and computation resources at the Center for Functional Nanomaterials, which is a U.S. Department of Energy Office of Science User Facility, and the Scientific Data and Computing Center, a component of the Computational Science Initiative, at Brookhaven National Laboratory, which are supported by the U.S. Department of Energy, Office of Basic Energy Sciences, under Contract No. DE-SC0012704. This research used resources of the National Energy Research Scientific Computing Center, a DOE Office of Science User Facility supported by the Office of Science of the U.S. Department of Energy under Contract No. DE-AC02-05CH11231.

REFERENCES

(1) Weitkamp, J. Zeolites and catalysis. *Solid State Ion.* **2000**, *131*, 175-188.
(2) Cundy, C. S.; Cox, P. A. The hydrothermal synthesis of zeolites: history and development from the earliest days to the present time. *Chem. Rev.* **2003**, *103*, 663-702.

(3) Knott, B. C.; Nimlos, C. T.; Robichaud, D. J.; Nimlos, M. R.; Kim, S.; Gounder, R. Consideration of the aluminum distribution in zeolites in theoretical and experimental catalysis research. *ACS Catal.* **2017**, *8*, 770-784.
(4) Li, Y.; Yu, J. New stories of zeolite structures: their descriptions, determinations, predictions, and evaluations. *Chem. Rev.* **2014**, *114*, 7268-7316.
(5) Pagis, C.; Morgado Prates, A. R.; Farrusseng, D.; Bats, N.; Tuel, A. Hollow zeolite structures: an overview of synthesis methods. *Chem. Mater.* **2016**, *28*, 5205-5223.
(6) Corma, A.; Diaz-Cabanas, M. J.; Martínez-Triguero, J.; Rey, F.; Rius, J. A large-cavity zeolite with wide pore windows and potential as an oil refining catalyst. *Nature* **2002**, *418*, 514-517.
(7) *http://www.iza-structure.org/databases/*.
(8) Smith, L. J.; Davidson, A.; Cheetham, A. K. A neutron diffraction and infrared spectroscopy study of the acid form of the aluminosilicate zeolite, chabazite (H-SSZ-13). *Catal. Lett.* **1997**, *49*, 143-146.
(9) Boscoboinik, J. A.; Shaikhutdinov, S. Exploring zeolite chemistry with the tools of surface science: challenges, opportunities, and limitations. *Catal. Lett.* **2014**, *144*, 1987-1995.
(10) Boscoboinik, J. A.; Yu, X.; Emmez, E.; Yang, B.; Shaikhutdinov, S.; Fischer, F. D.; Sauer, J.; Freund, H.-J. Interaction of probe molecules with bridging hydroxyls of two-dimensional zeolites: a surface science approach. *J. Phys. Chem. C* **2013**, *117*, 13547-13556.
(11) Wang, M.; Zhong, J.-Q.; Kestell, J.; Waluyo, I.; Stacchiola, D. J.; Boscoboinik, J. A.; Lu, D. Energy level shifts at the Silica/Ru (0001) heterojunction driven by surface and interface dipoles. *Top. Catal* **2017**, *60*, 481-491.
(12) Wang, M.; Zhong, J.-Q.; Stacchiola, D. J.; Boscoboinik, J. A.; Lu, D. First-Principles Study of Interface Structures and Charge Rearrangement at the Aluminosilicate/Ru (0001) Heterojunction. *J. Phys. Chem. C* **2018**, *123*, 7731-7739.
(13) Zhong, J.-Q.; Wang, M.; Akter, N.; Kestell, J. D.; Boscoboinik, A. M.; Kim, T.; Stacchiola, D. J.; Lu, D.; Boscoboinik, J. A. Immobilization of single argon atoms in nano-cages of two-dimensional zeolite model systems. *Nat. Commun.* **2017**, *8*, 16118.
(14) Schlexer, P.; Pacchioni, G.; Włodarczyk, R.; Sauer, J. CO adsorption on a silica bilayer supported on Ru (0001). *Surf. Sci.* **2016**, *648*, 2-9.
(15) Zhong, J. Q.; Wang, M.; Akter, N.; Kestell, J. D.; Niu, T.; Boscoboinik, A. M.; Kim, T.; Stacchiola, D. J.; Wu, Q.; Lu, D. Ionization‐facilitated formation of 2d (alumino) silicate–noble gas clathrate compounds. *Adv. Funct. Mater.* **2019**, *29*, 1806583.
(16) Büchner, C.; Lichtenstein, L.; Stuckenholz, S.; Heyde, M.; Ringleb, F.; Sterrer, M.; Kaden, W. E.; Giordano, L.; Pacchioni, G.; Freund, H.-J. Adsorption of Au and Pd on ruthenium-supported bilayer silica. *J. Phys. Chem. C* **2014**, *118*, 20959-20969.
(17) Janda, A.; Vlaisavljevich, B.; Lin, L.-C.; Smit, B.; Bell, A. T. Effects of zeolite structural confinement on adsorption thermodynamics and reaction kinetics for monomolecular cracking and dehydrogenation of n-butane. *J. Am. Chem. Soc* **2016**, *138*, 4739-4756.
(18) Van der Mynsbrugge, J.; Janda, A.; Mallikarjun Sharada, S.; Lin, L.-C.; Van Speybroeck, V.; Head-Gordon, M.; Bell, A. T. Theoretical analysis of the influence of pore geometry on monomolecular cracking and dehydrogenation of n-butane in Brønsted acidic zeolites. *ACS Catal.* **2017**, *7*, 2685-2697.
(19) Kresse, G.; Furthmüller, J. Efficient iterative schemes for ab initio total-energy calculations using a plane-wave basis set. *Phys. Rev. B* **1996**, *54*, 11169.

(20) Kresse, G.; Furthmüller, J. Efficiency of ab-initio total energy calculations for metals and semiconductors using a plane-wave basis set. *Comput. Mater. Sci.* **1996**, *6*, 15-50.
(21) Klimeš, J.; Bowler, D. R.; Michaelides, A. Chemical accuracy for the van der Waals density functional. *J. Phys. Condens. Matter* **2009**, *22*, 022201.
(22) Klimeš, J.; Bowler, D. R.; Michaelides, A. Van der Waals density functionals applied to solids. *Phys. Rev. B* **2011**, *83*, 195131.
(23) Lee, K.; Murray, É. D.; Kong, L.; Lundqvist, B. I.; Langreth, D. C. Higher-accuracy van der Waals density functional. *Phys. Rev. B* **2010**, *82*, 081101.
(24) Henkelman, G.; Uberuaga, B. P.; Jónsson, H. A climbing image nudged elastic band method for finding saddle points and minimum energy paths. *J. Chem. Phys.* **2000**, *113*, 9901-9904.
(25) McQuarrie, D. A.; Simon, J. D. *Molecular Thermodynamics*; Sterling Publishing Company, 1999.
(26) Bučko, T.; Benco, L.; Hafner, J.; Ángyán, J. G. Monomolecular cracking of propane over acidic chabazite: An ab initio molecular dynamics and transition path sampling study. *J. Catal.* **2011**, *279*, 220-228.
(27) Choomwattana, S.; Maihom, T.; Boekfa, B.; Pantu, P.; Limtrakul, J. Density functional theory study on catalytic cracking of n‐hexane on heteropoly acid: A comparison with acidic zeolite. *Can. J. Chem. Eng* **2012**, *90*, 865-872.
(28) Alaithan, Z. A.; Mallia, G.; Harrison, N. M. Monomolecular cracking of propane: effect of zeolite confinement and acidity. *ACS omega* **2022**, *7*, 7531-7540.
(29) Mallikarjun Sharada, S.; Zimmerman, P. M.; Bell, A. T.; Head-Gordon, M. Insights into the kinetics of cracking and dehydrogenation reactions of light alkanes in H-MFI. *J. Phys. Chem. C* **2013**, *117*, 12600-12611.
(30) Li, H.; Kadam, S. A.; Vimont, A.; Wormsbecher, R. F.; Travert, A. Monomolecular cracking rates of light alkanes over zeolites determined by IR operando spectroscopy. *ACS Catal.* **2016**, *6*, 4536-4548.
(31) Janda, A.; Vlaisavljevich, B.; Lin, L.-C.; Mallikarjun Sharada, S.; Smit, B.; Head-Gordon, M.; Bell, A. T. Adsorption thermodynamics and intrinsic activation parameters for monomolecular cracking of n-alkanes on Brønsted acid sites in zeolites. *J. Phys. Chem. C* **2015**, *119*, 10427-10438.
(32) Tranca, D. C.; Hansen, N.; Swisher, J. A.; Smit, B.; Keil, F. J. Combined density functional theory and Monte Carlo analysis of monomolecular cracking of light alkanes over H-ZSM-5. *J. Phys. Chem. C* **2012**, *116*, 23408-23417.
(33) Berger, F.; Rybicki, M.; Sauer, J. Adsorption and cracking of propane by zeolites of different pore size. *J. Catal.* **2021**, *395*, 117-128.
(34) Grimme, S. Semiempirical GGA‐type density functional constructed with a long‐range dispersion correction. *J. Comput. Chem.* **2006**, *27*, 1787-1799.
(35) Perdew, J. P.; Burke, K.; Ernzerhof, M. Generalized gradient approximation made simple. *Phys. Rev. Lett* **1996**, *77*, 3865.
(36) Perdew, J. P.; Burke, K.; Ernzerhof, M. Emission in symmetric heavy ion reactions at subthreshold energies. *Phys. Rev. Lett* **1997**, *78*, 1396.
(37) De Moor, B. A.; Reyniers, M.-F.; Marin, G. B. Physisorption and chemisorption of alkanes and alkenes in H-FAU: a combined ab initio–statistical thermodynamics study. *Phys. Chem. Chem. Phys* **2009**, *11*, 2939-2958.

(38) Piccini, G.; Alessio, M.; Sauer, J.; Zhi, Y.; Liu, Y.; Kolvenbach, R.; Jentys, A.; Lercher, J. A. Accurate adsorption thermodynamics of small alkanes in zeolites. Ab initio theory and experiment for H-chabazite. *J. Phys. Chem. C* **2015**, *119*, 6128-6137.
(39) Barrer, R. M.; Davies, J. Sorption in decationated zeolites ii. Simple paraffins in h-forms of chabazite and zeolite l. *Proc. R. Soc. Lond. A: Math. Phys. Sci.* **1971**, *322*, 1-19.
(40) Kadam, S. A.; Li, H.; Wormsbecher, R. F.; Travert, A. Impact of zeolite structure on entropic–enthalpic contributions to alkane monomolecular cracking: an IR operando study. *Chem. Eur. J.* **2018**, *24*, 5489-5492.
(41) Chehaibou, B.; Badawi, M.; Bucko, T.; Bazhirov, T.; Rocca, D. Computing RPA adsorption enthalpies by machine learning thermodynamic perturbation theory. *J. Chem. Theory Comput* **2019**, *15*, 6333-6342.
(42) Göltl, F.; Hafner, J. Modelling the adsorption of short alkanes in protonated chabazite: The impact of dispersion forces and temperature. *Microporous Mesoporous Mater.* **2013**, *166*, 176-184.
(43) Cored, J.; Wang, M.; Akter, N.; Darbari, Z.; Xu, Y.; Karagoz, B.; Waluyo, I.; Hunt, A.; Stacchiola, D.; Head, A. R. Water Formation Reaction under Interfacial Confinement: Al0. 25Si0. 75O2 on O-Ru (0001). *Nanomaterials* **2022**, *12*, 183.
(44) Wang, M.; Zhou, C.; Akter, N.; Tysoe, W. T.; Boscoboinik, J. A.; Lu, D. Mechanism of the accelerated water formation reaction under interfacial confinement. *ACS Catal.* **2020**, *10*, 6119-6128.
(45) Bučko, T.; Hafner, J. The role of spatial constraints and entropy in the adsorption and transformation of hydrocarbons catalyzed by zeolites. *J. Catal.* **2015**, *329*, 32-48.
(46) Van der Mynsbrugge, J.; Janda, A.; Lin, L. C.; Van Speybroeck, V.; Head‐Gordon, M.; Bell, A. T. Understanding Brønsted‐Acid Catalyzed Monomolecular Reactions of Alkanes in Zeolite Pores by Combining Insights from Experiment and Theory. *ChemPhysChem* **2018**, *19*, 341-358.
(47) Zimmerman, P. M.; Tranca, D. C.; Gomes, J.; Lambrecht, D. S.; Head-Gordon, M.; Bell, A. T. Ab initio simulations reveal that reaction dynamics strongly affect product selectivity for the cracking of alkanes over H-MFI. *J. Am. Chem. Soc* **2012**, *134*, 19468-19476.
(48) de Oñate Martínez, J.; McCusker, L. B.; Baerlocher, C. Characterization and structural analysis of differently prepared samples of dehydrated VPI-5. *Microporous Mesoporous Mater.* **2000**, *34*, 99-113.
(49) Wang, G.; Marler, B.; Gies, H.; Fyfe, C. A.; Sidhu, P.; Yilmaz, B.; Müller, U. Synthesis, characterization and structure analysis of UZM-22, a MEI-type zeolite framework structure. *Microporous Mesoporous Mater.* **2010**, *132*, 43-53.
(50) Benazzi, E.; Leite, L.; Marchal-George, N.; Toulhoat, H.; Raybaud, P. New insights into parameters controlling the selectivity in hydrocracking reactions. *J. Catal.* **2003**, *217*, 376-387.
(51) Sabater, M. J.; Sastre, G. A computational study on the templating ability of the trispyrrolidinium cation in the synthesis of ZSM-18 zeolite. *Chem. Mater.* **2001**, *13*, 4520-4526.
(52) Butler, I. S.; Harrod, J. F. *Inorganic chemistry: principles and applications*; Benjamin-Cummings Publishing Company, 1989.

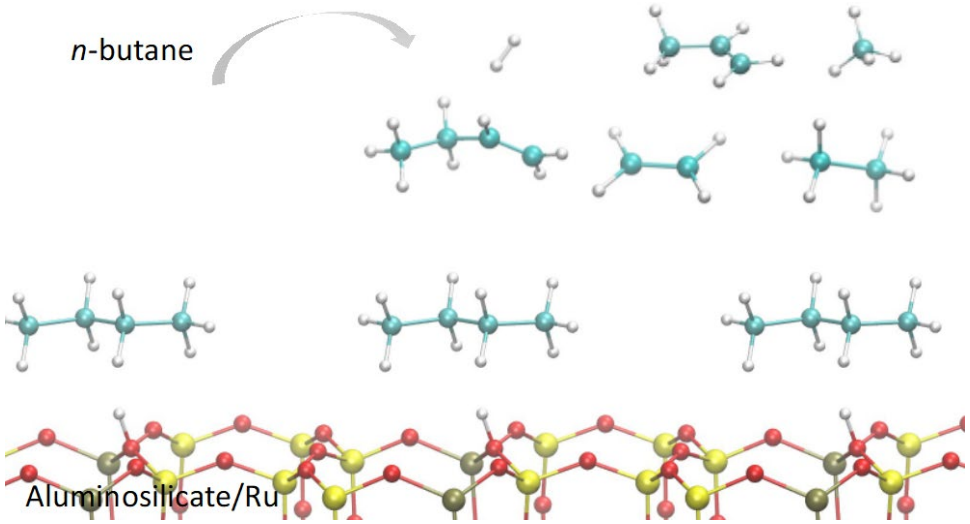

TOC Graphic